Isothermal Crystallization of Nylon-6/Montmorillonite Nanocomposites

Derek M. Lincoln† and Richard A. Vaia*

Air Force Research Laboratory, Materials and Manufacturing Directorate, Wright-Patterson AFB, Ohio 45433-7750

Ramanan Krishnamoorti

Department of Chemical Engineering, University of Houston, Houston, Texas 77004-4004

Received February 3, 2004; Revised Manuscript Received April 10, 2004

ABSTRACT: The isothermal crystallization of in-situ-polymerized and melt-processed nylon-6/montmorillonite nanocomposites was studied by simultaneous small- and wide-angle X-ray scattering using synchrotron radiation. The isothermal crystallization rates, in the nucleation-controlled regime, for the nanocomposites are significantly faster than that for the pristine nylon-6 and suggest that the layered silicates act as nucleating centers. Within the experimental resolution, the initial crystal phase formed between 185 and 205 °C in the presence of the layered silicate is the metastable γ-phase, whereas the α-phase develops in the pristine nylon-6 at comparable temperatures. Additionally, the strong silicate−polymer interactions present in the in-situ-polymerized nanocomposites alter the crystallization process, creating a much weaker temperature dependence for the crystallization kinetics. Finally, the presence of well-dispersed layered silicates significantly disrupts the development of lamellar structure but does not alter the overall amounts of crystallinity.

1. Introduction

Filled polymers are found in a number of industrial and commercial areas including automotive, electrical, industrial HVAC components, power tools, pulley, and gears. Use stems from enhancement of physical properties and the addition of filler-specific characteristics as well as reduced resin volume and thus cost. Industrially useful examples exhibit increases of tensile strength up to 25%, flexural modulus up to 100%, and impact strength up to 100%.[1] They also display low shrinkage upon secondary processing and high heat distortion temperature.[2]

Polymer-layered silicate nanocomposites (PLSN) challenge traditional filled polymers (loadings of 20 wt % or more) in many of these areas by providing similar physical enhancements but with as little as 5 wt % addition of dispersed, 1 nm thick aluminosilicate layers (diameters of layers commonly ranging from 20 (laponite) to 500 nm (representative montmorillonite)).[3] Previous PLSN reports include increased modulus,[4,5] impact strength,[4,6] heat distortion temperature (HDT),[4,5] and barrier properties[7−9] with decreased thermal expansivity.[10] In addition, PLSNs are finding new applications due to their reduced flammability,[11] resistance to UV degradation,[12] resistance to atomic oxygen,[13,14] and improved ablative performance.[15] Various review articles provide summaries of the structure of layered silicates, approaches to synthesis, and property enhancements.[16−18]

Up to recently, the vast majority of research and development has been focused on the synthesis of PLSNs from commodity resins, including polyolefins,[19,20] polyamides,[4,9,14,15,21] polymethacrylates,[22] polystyrenes,[8,23] epoxies,[24] and elastomers,[25] and determination of the subsequent property enhancements. The general conclusion drawn from more than 20 years of these efforts is that not all resin systems display the same property enhancements; thus, the fundamental principles governing PLSNs are more complex than embodied in a system-independent, idealized, schematic morphology of rigid plates randomly arranged in a continuum. Issues such as detailed characterization of the dispersion,[26−29] quantifiable and controllable interfacial interactions,[30] local dynamics of the polymer at the interface,[31] thermal stability,[32,33] physically correct structure−mechanics relationships,[34] and alteration of polymer crystallization and crystallite morphology are currently critical areas of intense investigation.

In general, low volume percent (1−5 vol %) addition of layered silicate impacts polymer crystallite development, having been observed in the vast majority of investigations on semicrystalline polymer PLSNs, including polypropylene−maleic anhydride polypropylene,[35,36] poly(L-lysine),[37] PET,[38,39] sulfo-PET,[38] syndiotactic polysytene,[40,41] poly(ethylene−vinyl acetate),[42] poly(ethylene oxide),[43] poly(vinyl alcohol),[44] and polyamides (6,6;[45] 10,10;[46] 12,12[47]). Nylon-6 nanocomposites[4,48−56] have been the most extensively studied semicrystalline nanocomposite to date, greatly facilitated by the substantial investigations available on the unfilled polymer. An abbreviated review of current literature is included as Supporting Information. General effects include induced polymorphism,[35,40,44−46,48−50] small, irregular crystallites (dendrites, hedrites),[36,39,44,51] increased crystallization rate,[37−39,45,46,50,52,53] and alteration of the crystal fraction.[40,41,54] The extent of these effects depends on process history and specific characteristics of the resin. For example, the impact of layered silicate addition on the nucleation and growth rate has been ascribed to the biasing of chain conformation near the interface,[40,41,51] a decrease of the activation barrier to nucleation,[38,46] and the alteration of chain mobility.[36,37,45,55] Both enhancement of interfacial mobility−

† Current address: United States Air Force Academy, Department of Chemistry, USAFA, CO 80840.

* Corresponding author: e-mail richard.vaia@wpafb.af.mil; fax (937) 255-9157.

10.1021/ma049768k CCC: $27.50
Published on Web 05/21/2004

due to increased free volume at the polymer−layer interface or partial solublization of interfacial polymer chains by surfactant or degradation products—and retardation of interfacial mobility—due to specific hydrogen bonding,[49,55] coordination,[37] or electrostatic interactions[36] between the polymer and surface—have been discussed. Overall, deconvoluting the relative roles and influence of stress, temperature history, and small molecular impurities, either purposely (epoxy) or inadvertently (degradation and unexchanged surfactants) added, on crystallization in nanocomposites is not fully understood. Comprehensive investigations are challenging owing to the sensitivity of nucleation and growth to process history and lack of sufficiently quantitative techniques to describe nanofiller morphology (dispersion, orientation, local concentration).

The observations for PLSNs parallel the behavior of blends and filled semicrystalline polymers, where the increased interfacial area alters the energetics and kinetics of nucleation and growth, and thus the crystallite fraction, morphological organization, and at times even phase. The result is a profound impact on the mechanical properties of the composite. For example, the morphology (size, shape, and distribution) of spherulites dictates fracture behavior and toughness. Likewise, different crystal phases exhibit different mechanical properties—the γ phase of nylon-6 was shown to be less rigid and more ductile than the α phase.[56]

In this paper the influence of dispersed layered silicate on the morphological development during isothermal crystallization of nylon-6 is discussed toward providing insight into the origin of morphological differences between semicrystalline polymers and their corresponding PLSNs as well as providing a baseline for process guidelines to enable control of the polymer crystallite fraction and morphology in these PLSNs. Simultaneous small-angle (crystal lamellae) and wide-angle (crystalline regions) X-ray scattering during isothermal quenches from the melt for in-situ-polymerized and melt-processed nylon-6 nanocomposites provides insight into the influence of the concentration of layered silicate, polymer-layered silicate interaction, and polymer molecular weight on the temperature dependence of the morphology development of the crystalline regions of nylon-6.

2. Experimental Section

2.1. Materials. Commercially available 2 wt % (NCH2) and 5 wt % (NCH5) layered silicate/nylon-6 in-situ-polymerized PLSN materials and pure nylon-6 polymer (Nyl6) were obtained from Ube Industries, Ltd. (Japan).[57] Ring-opening polymerization of ϵ-caprolactam initiated by the pendant carboxylic acids on the surface of the modified montmorillonite reportedly results in approximately 50% (NCH5) and 30% (NCH2) of the nylon-6 chains "tethered" to the surface of the montmorillonite via ionic interaction of the primary ammonium cation.[57] The resultant weight-average molecular weights of the nylon-6 polymer in PLSN are 22 200 (NCH2) and 19 700 g/mol (NCH5), respectively.[58] A melt-processed nylon-6 PLSN obtained from Southern Clay Products (Gonzalez, TX) was also examined.[59] In contrast to the in-situ-polymerized material, weak secondary interactions, such as hydrogen-bonding and dispersive interactions, dominate the polymer−silicate interactions in the melt-processed NLS4. Previous scattering and microscopy investigations have indicated that these PLSN systems qualitatively have comparable degrees of dispersion.[59,60]

Extruded pellets of the PLSNs were dried under vacuum at 70−80 °C for 3−4 h prior to compression-molding into 7 mm circular disks, ∼1 mm thick. Platens of a hydraulic press were preheated to ∼280 °C. The mold containing pellets was placed between the platens and allowed to heat to ∼240 °C for several minutes before 500 lbs of force was applied. The force was kept constant as the mold was heated gradually to ∼230−240 °C over approximately 12 min. The mold was removed, placed on a room temperature steel heat sink, and allowed to cool to room temperature in the ambient. This provided the initial process state for compression-molded samples.

2.2. X-ray Characterization. Simultaneous small-angle (SAXS) and wide-angle (WAXS) X-ray scattering experiments were conducted at the Advanced Polymers Beamline (X27C) of the National Synchrotron Light Source (NSLS), Brookhaven National Laboratory (BNL). The wavelength of the incident X-rays was 1.307 Å defined by a double multilayer monochromator. The synchrotron X-rays were collimated to a 600 μm beam size using a three-pinhole collimator.[61] Data were collected using two linear position-sensitive detectors[62] at 190 cm (SAXS) and 20 cm (WAXS). The scattering angle was calibrated using silver behenate (SAXS) and quartz (WAXS) powder samples. Samples, mounted in copper holders, were placed in a small temperature chamber at ∼250 °C for approximately 5 min. The samples were then pneumatically shuttled to another small temperature chamber in the beam at the indicated crystallization temperature and for the indicated time duration. Details of the dual-chamber temperature jump apparatus can be found elsewhere.[61] Data acquisition times varied from 0.25 to 4 min per scan, increasing in duration as the rate of change of the scattering pattern decreased. All the X-ray data were corrected for beam fluctuations and sample absorption.

Deconvolution of the superposition of crystalline and amorphous peaks observed in the WAXS data was carried out using the nonlinear least-squares routine within Genplot X-Window Interface Data Analysis and Plotting Package for Scientists and Engineers (Computer Graphic Service). A 2θ range 8°−28° was selected to include all the intense crystalline and amorphous peaks of nylon-6. The baseline was defined by a linear fit to the first and last six data points. Pearson VII peaks converged during optimization to Gaussian. Thus, Gaussian peaks yielded smaller residual than Lorentzian and were used to describe both amorphous and crystalline reflections. The analyses yielded integrated intensities, positions, heights, and widths of the various reflections. The temporal data series were processed in a batch mode. Typically, the last scan in the temporal series was analyzed iteratively to determine the optimum parameters (height, position, and width) of the various peaks. The remaining scans were then deconvoluted sequentially (decreasing time) using the optimized parameters from the previous scan as the initial parameters for the next optimization.

The crystalline index, CI, is defined as the ratio of the total intensity of crystalline reflections to the total observed intensity (crystalline + amorphous) and is normalized to the maximum crystalline index observed for each individual sample at the corresponding crystallization temperature. The induction time, t_i, was determined by the intercept of a linear fit of the primary crystallization regime with CI = 0. The initial crystallization rate was the slope of the aforementioned linear fit. The half-crystallization time, $t_{1/2}$, was determined as $(t_e - t_i)/2$, where t_e is the end of the primary crystallization regime determined by the intersection of the linear fit for the initial crystallization and secondary crystallization. Finally, the crystallite size and perfection (defect concentration within the crystallites) were determined from the Scherrer equation ($L_{hkl} = 0.9\lambda/(\text{fwhm} \times \cos(\theta_{hkl}))$, where λ is the X-ray wavelength (1.307 Å) and fwhm is the full width at half-maximum in radians of the hkl reflection at 2θ.[63]

3. Results and Discussion

3.1. Crystalline development of Nylon-6 and Nanocomposites. The temporal development of the wide-angle X-ray scattering (WAXS) at 200 °C for

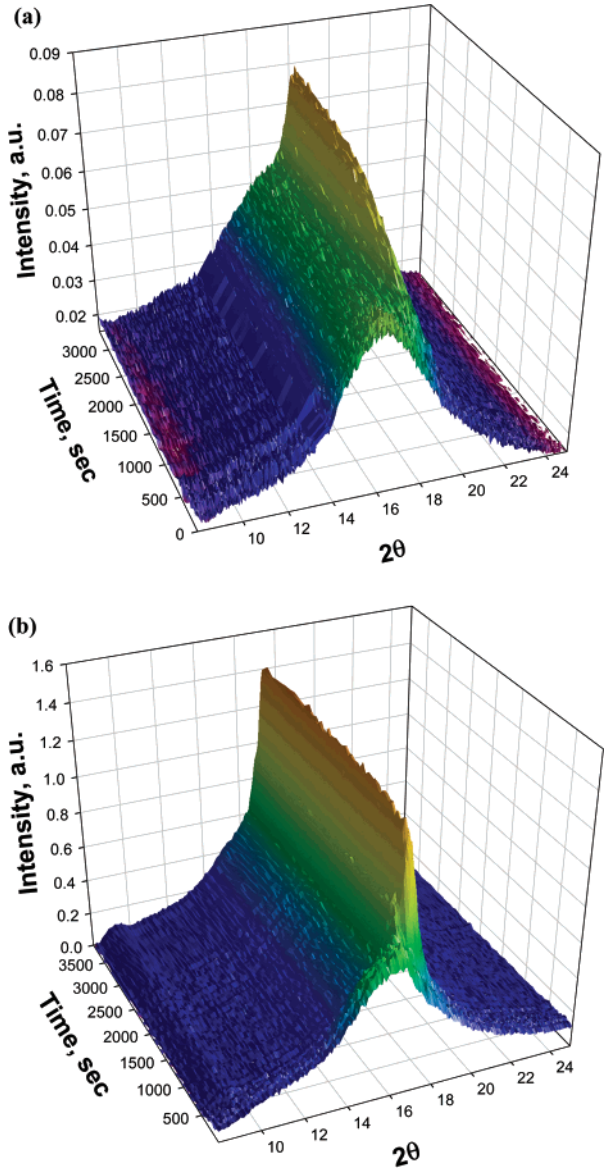

Figure 1. Temporal development of the wide-angle X-ray scattering at 200 °C for (a) nylon-6 and (b) NCH5 quenched from the melt (250 °C). $t = 0$ s corresponds to the insertion of the molten sample into the equilibrated crystallization furnace. These data sets are typical of the scattering data from the isothermal crystallization experiments of nylon-6, NCH2, NCH5, and NLS4 between 180 and 205 °C.

nylon-6 and NCH5 quenched from the melt (250 °C) is summarized in Figure 1. Time $t = 0$ s corresponds to the insertion of the molten sample into the equilibrated crystallization furnace. These data sets are typical of the scattering data for the isothermal crystallization experiments of nylon-6, NCH2, NCH5, and NLS4 between 180 and 205 °C. Experimental observations closer to the melting temperature ($T_m = 225$ °C) were limited by very slow structure development, whereas temperatures lower than 180 °C were limited by finite temporal resolution of the data collection ($t \sim 5$ s) and obtainable equilibration times ($t \sim 10$ s at 185 °C) within the crystallization furnace being greater than the crystallization rates.

Qualitatively, a broad peak ($2\theta \sim 16.3°$), reflecting scattering from amorphous chains in the melt, rapidly gives way to a narrow feature ($2\theta \sim 17.4°-18.4°$) arising from chain−chain correlation in crystalline domains. The increase of the crystalline scattering intensity directly corresponds to the increase in the volume fraction of crystallites. Representative WAXS data of nylon-6 and NCH5 near completion of crystallization at 200 °C and the associated deconvolutions are shown in Figure 2. For nylon-6, peak deconvolution required one broad peak ($2\theta \sim 16.1°$), ascribed to the amorphous phase, and two smaller, narrower peaks ascribed to the α-crystalline phase with $\alpha_1(2\theta = 16.0°)$ and $\alpha_2(2\theta = 18.5°)$ corresponding to the 200 and 002/202 reflections, respectively.[64] In agreement with previous isothermal and nonisothermal in-situ X-ray studies of nylon-6,[48,66,67] the relative d spacing of 200 and 002/202 converge with increasing temperature, reflecting an increase in the chain−chain spacing within the hydrogen-bonded sheet and a contraction in the separation of the hydrogen-bonded sheets within the monoclinic α-crystallites at elevated temperature. The change in d spacing is not linear with temperature, and paralleling nylon-6,6, has been associated with a Brill transition between 120 and 180 °C, separating a room temperature monoclinic α phase and an elevated temperature monoclinic α′ phase.[66,67]

For all the nanocomposites, at all temperatures examined, the WAX data were described by one amorphous ($2\theta \sim 17.0°$) and one crystalline peak ($2\theta \sim 17.5°$), ascribed to the 001 reflection of the γ phase.[64] Despite the high temperature of crystallization, the WAX profile of NCH5 at 200 °C closely resembles that observed at room temperature for NCH5 nanocomposites.[4] The relatively temperature-insensitive chain−chain separation in the pseudohexagonal γ-phase is consistent with previous in-situ X-ray scattering studies.[48,66] The development of the γ-phase even at temperatures near the melting point, and throughout the isothermal crystallization process, indicates that the presence of the layered silicates dominate the driving force favoring γ formation. Correspondingly, previous nonisothermal WAX investigations of crystalline melting revealed the dominate crystal phase in the nanocomposites at temperatures greater than 180 °C was γ, implying the presence of the layered silicate also dominates the energetics of γ-phase stability.[48]

The development of the normalized crystalline index ($\overline{CI}$) during isothermal crystallization (185, 190, 195, 200, and 205 °C) of nylon-6 and the various nanocomposites (NCH2, NCH5, and NLS 4) is shown in Figure 3. $\overline{CI} = CI(t)/CI(t\rightarrow\infty)$, where $CI(t\rightarrow\infty)$ is the final, maximum CI for crystallization process and is summarized for the various samples and conditions in Table 1. The final crystalline index was between 0.18 and 0.26. This is slightly lower (~0.05) than reported for comparable materials and temperatures during heating ramps up to the melting temperature.[48] Note that absolute CI values depend on data analysis procedures (background removal and mathematical description of reflection). Overall, no major systematic trends of $CI(t\rightarrow\infty)$ with layered silicate loading or crystallization temperature were observed. In general, this is consistent with numerous literature reports that the layered silicates have only a minor impact on the total crystalline fraction of nylon-6 (see Supporting Information). Greater temperature resolution would be necessary to determine whether there is an intermediate crystallization temperature that consistently provides a greater degree of crystallinity for the nanocomposites.

To compare the various samples and crystallization temperatures, the induction time, initial crystallization

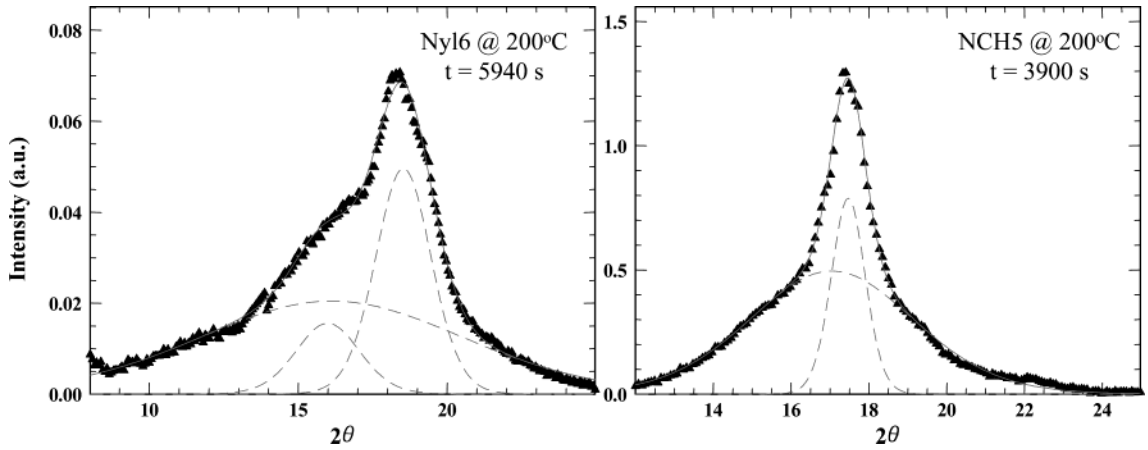

Figure 2. Profile-fitted WAXS data near the completion of isothermal crystallization at 200 °C for (a) Nyl6 (t = 5940 s) and (b) NCH5 (t = 3900 s). The fitted data are the sum of the components shown by dashed lines. Linear background was removed before deconvolution. Similar data were obtained for the various isothermal crystallization experiments.

rate, and half-crystallization time derived from the data in Figure 3 are summarized in Figures 4, 5, and 6, respectively.

The time until the initial observation of the crystalline reflection(s) is the induction time, t_i, ideally reflecting the time needed to form a critical nucleus. In the current experiments this induction time is convoluted with the time necessary to achieve thermal equilibrium at the crystallization temperature in the crystallization furnace. Additionally, this equilibration time will change with the isothermal crystallization temperature and will increase with decreased crystallization temperature (greater temperature quench). Assuming that the low volume fraction addition of layered silicate does not alter the thermal conductivity and heat capacity of the nylon-6, the time−temperature profile will be the same for the various samples at a given crystallization temperature, enabling comparisons of t_i, even though rigorous quantitative discussion of the absolute values is somewhat compromised. Nylon-6 has the longest induction times at all crystallization temperatures and exhibits a minimum at intermediate temperatures (190 °C) (Figure 4). The minimum arises from a competition between an increase in the thermodynamic driving force for nucleation and a decrease in the kinetic mobility of the polymer with greater quench depths ($T_m - T_c$). The melt-processed NLS4 has the shortest average induction times of the nanocomposites examined and also exhibits a minimum at intermediate temperatures. In contrast, the induction times for the in-situ-polymerized NCH2 and NCH5 fall between those of nylon-6 and NLS4 and exhibit reduced temperature sensitivity. Recall that although NLS4 exhibits shorter induction times than NCH5, it contains less layered silicate with arguably poorer dispersion, implying less polymer-layered silicate interfacial area.[60] The overall behavior implies that the characteristics of the polymer-layered silicate interaction, especially when strong such as for NCH2 and NCH5, fundamentally alter the nature of the crystallization process, as noted previously by the changed crystalline morphology.

The initial crystallization rate for all systems increases as the crystallization temperature decreases (Figure 5). This indicates a nucleation-controlled growth regime, as depicted in the inset. At 205 °C, the crystallization rates of the nanocomposites are approximately similar and greater than pure nylon-6. As the crystallization temperature is decreased, the in-situ-polymerized systems (NCH2 and NCH5) crystallize much faster than NLS4.

This behavior is mirrored in the behavior of the half-crystallization time, $t_{1/2}$[68] (Figure 6). We note that much of the uncertainty associated with the convolution of the equilibration and nucleation processes for the induction time is largely eliminated in the comparison of the half-crystallization time and allows for a more quantitative comparison. Decreased crystallization temperature decreases $t_{1/2}$, and in-situ-polymerized NCH2 and NCH5 exhibit shorter $t_{1/2}$'s than observed for melt-processed NLS4 for all crystallization temperatures. For example, even though NLS4 has nearly twice the concentration of layered silicate than NCH2, it exhibits longer $t_{1/2}$'s.

The relative effects of layered silicate on the initial crystallization rate and $t_{1/2}$, where stronger interactions increases the rate of crystal formation, somewhat contrast with the trends observed for induction times. Tethering the chains may retard critical nucleus formation at the layered silicate−polymer interface, but once established provides favorable conditions for greater growth rates. The restricted chain motion or nonequilibrium surface chain density arising from end-tethering of the polymer at the layered silicate surface could inhibit optimal formation of a critical nucleus; however, once the initial energy barrier to nucleation is overcome, the increased fraction of parallel chain−chain conformations may enhance growth of γ at the interface. Additionally, melt-processing of the nylon-6 nanocomposites in the presence of organically modified layered silicates might also result in significant chain length degradation that might also suggest a shorter induction time. Nevertheless, future investigations are necessary to determine the relative importance of thermodynamic factors, such as biased chain conformation (chains preferentially parallel orientation because of the surface-initiated polymerization process), and kinetic factors, such as increased breadth of relaxation modes in the proximity of the layered silicate, to the nucleation and subsequent growth processes.

Figure 7 summarizes the crystallite size and perfection, L_{hkl}, with regard to the Scherrer equation for the γ reflection ($2\theta_{001} = 17.5°$) of the nanocomposites and the α_1 and α_2 reflections ($2\theta_{200} = 16.0°$; $2\theta_{002/202} = 18.5°$) of nylon-6 at the terminus of isothermal crystallization. The narrower the X-ray reflection, the greater the extent of spatial correlations between scattering planes. Con-

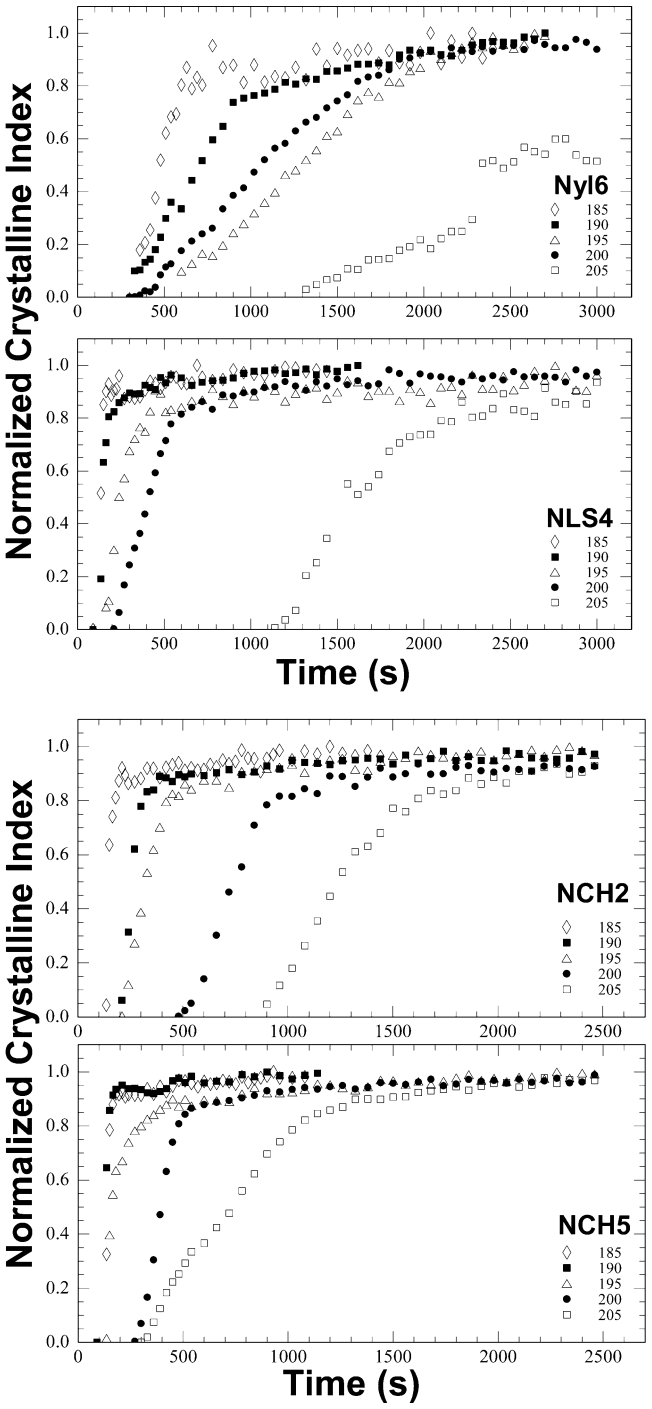

Figure 3. Development during isothermal crystallization (185, 190, 195, 200, and 205 °C) of the normalized crystalline index ($\overline{CI}$) for Nyl6, NCH2, NCH5, and NLS 4. $\overline{CI} = CI(t)/CI(t\rightarrow\infty)$, where $CI(t\rightarrow\infty)$ is summarized in Table 1.

Table 1. Maximum Values of the Crystalline Index, $CI(t\rightarrow\infty)$

	185 °C	190 °C	195 °C	200 °C	205 °C
Nyl6	0.24	0.26	0.23	0.23	(0.14)[a]
NCH2	0.20	0.17	0.22	0.20	0.22
NCH5	0.26	0.30	0.23	0.26	0.26
NLS4	0.26	0.26	0.20	0.20	0.18

[a] Extrapolated value. Crystallization was not complete at terminus of experiment. $t_{1/2}$ and crystallization rate are thus approximate.

ventionally, enhanced nucleation density and increased growth rates are expected to produce smaller, less

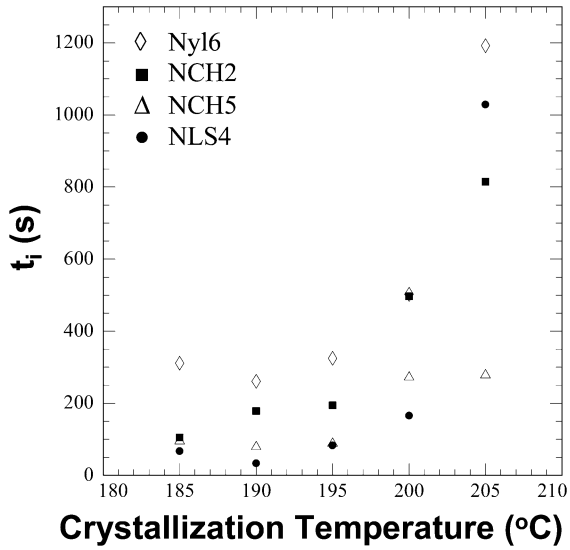

Figure 4. Induction time, t_i, for the onset of crystallization.

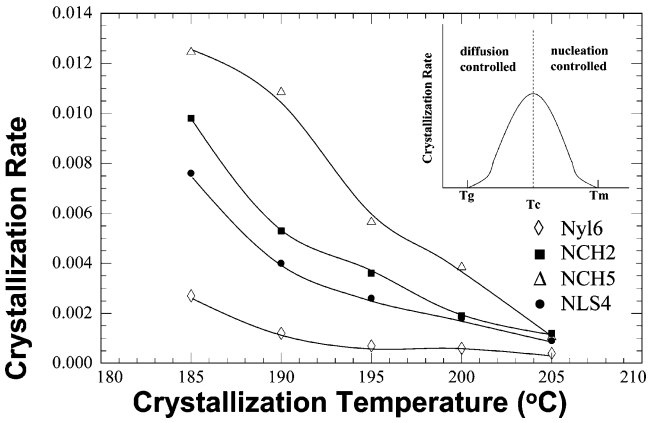

Figure 5. Initial crystallization rate.

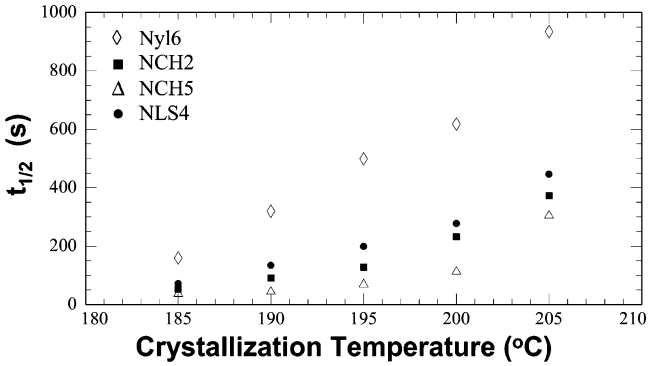

Figure 6. Half-crystallization time, $t_{1/2}$.[68]

perfect polymer crystallites and thus broader reflections. For the nanocomposites though, the L_{hkl} is substantially greater (reflections narrower) than for pure nylon-6. The higher symmetry (pseudohexagonal) of the γ phase should result in greater energetic equivalence between the growth surfaces normal to the chain backbone ((001), (011), and (010)). Thus, the γ phase is anticipated to inherently exhibit longer range correlations within the crystallite. Additionally though, the L_{hkl} of the nanocomposites increase with increasing silicate content. The impact per volume fraction of layered silicate is greater as the isothermal crystallization temperature nears the melting temperature. While it is expected that the layer silicate surface must exert significant influence

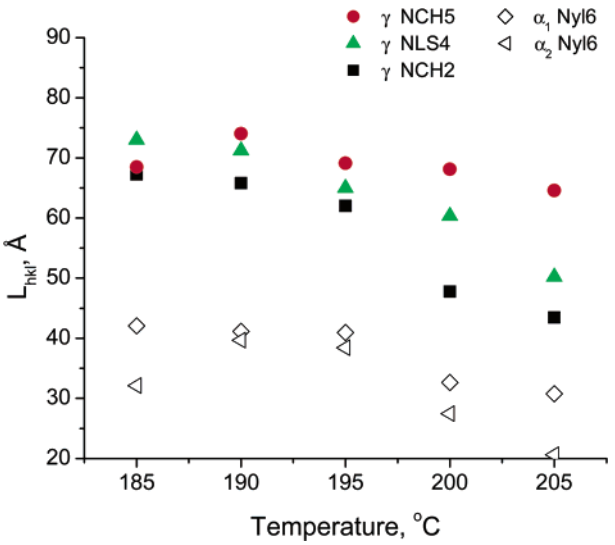

Figure 7. Crystallite size and perfection, L_{hkl}, with regard to the Scherrer equation for the γ reflection ($2\theta_{001} = 17.5$) of the nanocomposites and the α_1 and α_2 reflections ($2\theta_{200} = 16.0°$; $2\theta_{002/202} = 18.5°$) of nylon-6 at the terminus of isothermal crystallization. $L_{hkl} = 0.9\lambda/(\text{fwhm} \times \cos(\theta))$, where λ is the X-ray wavelength (1.307 Å) and fwhm is the full width at half-maximum in radians of the *hkl* reflection at 2θ.

on the extent of chain ordering, the specific mechanisms of such ordering are not obvious.

3.2. Lamellar Morphology Development of Nylon-6 and Nanocomposites. Contour small-angle X-ray scattering intensity plots for crystallization at 205 °C of nylon-6 and NCH5 are presented in Figure 8. For nylon-6, a distinct peak at $q = 0.41$ nm^{-1} and increased scattered intensity at low q values developed as crystallization proceeds. The peak position of the scattered intensity corresponds to the repeat distance of the crystalline lamellae. In contrast, an increase in intensity, especially at the low q, and no additional development of features such as a scattering maximum occur during isothermal crystallization of NCH5.

Overall, the time-dependent changes in the scattered intensity in this region of reciprocal space mirrors the development of structure determined from WAXS and summarized by $\overline{\text{CI}}$ in Figure 3. Determination of the initial event, i.e., development of chain−chain correlations or long-range lamellae fluctuations, as well as any phase lag between the structure development of the lamellae and ordering within the crystallites was compromised by the complexity of the small-angle scattering profiles of the nanocomposites, insufficient temporal resolution at the onset of crystallization and inability to access lower q values.

Figure 9 compares the SAXS data for nylon-6 and the nanocomposites in the melt state before quenching and after crystallization at 205 °C. As reported previously,[48] the nanocomposites have comparable levels of crystallinity (as interpreted by WAXD), but little of that material is incorporated into lamellae structures presumably due to disruption of such long-ranged order structures by the presence of the silicate layers.

The melt profiles clearly demonstrate that with increasing silicate content there is additional scattered intensity at low q, which is attributed to the larger number of scattering entities (i.e., silicate sheets or their aggregates). On the other hand, for the samples crystallized at 205 °C, as the silicate content increases, the resolution (width and intensity) of the lamellae reflection decreases. Beyond steeper background scattering arising from the dispersed silicate layers, the mesoscopic crystalline structure of NCH2 is similar to that of pure nylon-6. For NLS4, the disruption in the lamellar structure is apparent, reflected as an intensity decrease and broadening of the reflection at $q = 0.437$ nm^{-1} ($d = 14.4$ nm). Additionally, substantially increased low q, featureless scattered intensity develops, indicating a more disordered, hierarchical morphology relative to that of pure nylon-6. This is consistent with a greater nucleation density and faster crystallization processes, producing crystallites with a greater distribution of size and shape. Finally, NCH5 exhibits the greatest disruption of the mesoscale structure and does not develop a well-defined scattering maximum indicative of a lamellar spacing. During crystallization, only an increase of featureless scattering, without scattering maxima, at low q values was observed. In addition, reflections at $q = 0.302$ nm^{-1} ($d = 20.8$ nm) and $q = 0.158$ nm^{-1} ($d = 39.8$ nm) persist from the melt state (and similar to those reported using SAXS in the equilibrium melt state

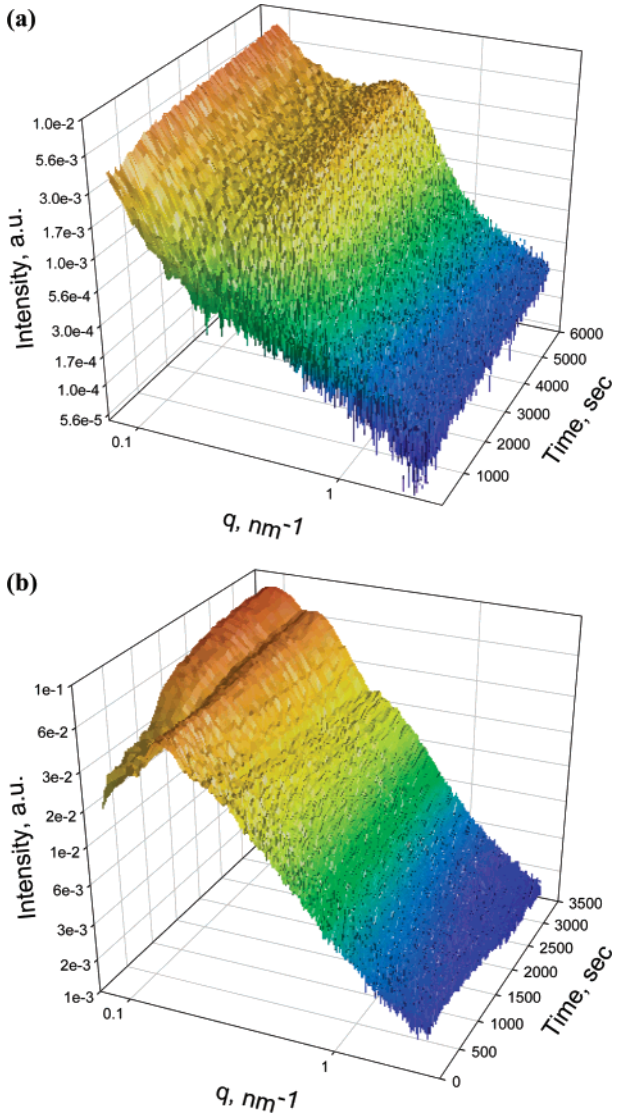

Figure 8. Small-angle X-ray scattering (SAXS) data at 205 °C for (a) nylon-6 and (b) NCH5. Note that the abscissa and intensity axes are logarithmic. $t = 0$ s corresponds to the insertion of the molten sample into the equilibrated crystallization furnace. These data sets are typical of the scattering data from the isothermal crystallization experiments of nylon-6, NCH2, NCH5, and NLS4 between 180 and 205 °C.

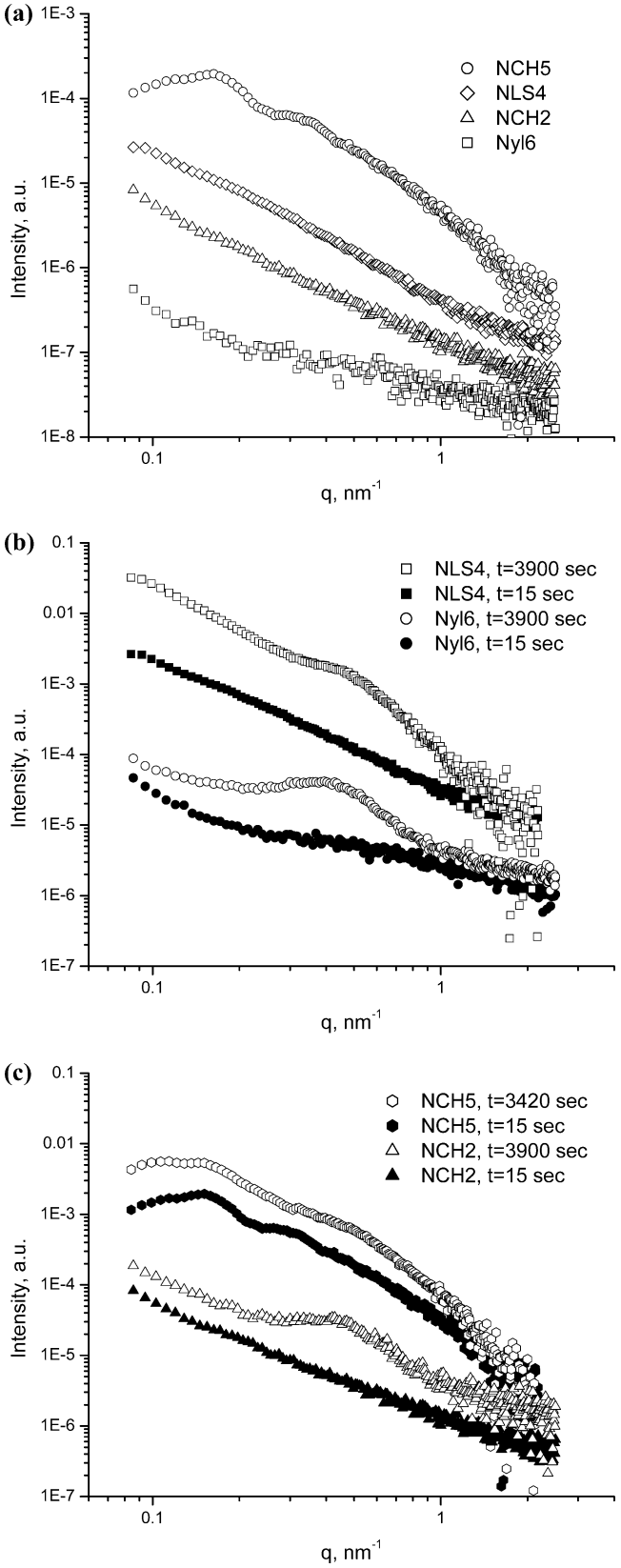

Figure 9. Small-angle X-ray scattering (SAXS) data for nylon-6, NCH2, NCH5, and NLS4 (a) before crystallization and at the onset and terminus of crystallization for (b) Nyl6 and NLS4 and for (c) NCH2 and NCH5 at 205 °C. Note that the scattering pattern for NCH5 did not markedly change after 2000 s, and data collection was terminated at 3400 s. The data sets are offset for viewing.

at 250 °C[60]) through the entire crystallization process. Estimates of the mean layer−layer spacing for a fully exfoliated 5 wt % nanocomposite exhibiting a nematic arrangement agree with the SAXS and TEM results showing layer−layer correlations with a correlation length of ∼40 nm.[60] The persistence of these feature throughout the crystallization processes implies that crystallization in NCH5 does not disturb the relative distribution of layered silicates and lends further credence to the previously observed disturbance to the long-range lamellar order of the polymer crystals by a uniform distribution of the layered silicates.

4. Conclusions

Simultaneous small- and wide-angle X-ray scattering-based isothermal crystallization studies of nylon-6-based nanocomposites using synchrotron radiation has provided significant insight into the factors controlling the development of crystalline structure and the interplay between the effective mesoscale dispersion of the nanoscale highly anisotropic layers and the development of local and long-range crystalline order. It has been demonstrated quantitatively that the silicate layers act as nucleating centers, and when there are strong interactions between the silicate sheets and the polymer, significant changes in the morphological structure (unit cell) of the crystals along with the crystallization kinetics are also observed. However, the effect of the silicate sheets on the long-range lamellar order is somewhat less conclusive, in part, because of the inability to separate the contributions to the low-q scattering arising from fluctuations in the polymer melt, structure, and dispersion of the silicate layers and the development of crystalline order. X-ray experiments where we access lower q values, small-angle neutron scattering with a small fraction of deuterium-labeled chains, and real-time FTIR measurements, among others, might help sort out some of these issues along with outstanding questions regarding the relative importance of thermodynamic factors, chain conformations, chain mobility, and other kinetic factors on the crystallization in such polymer nanocomposites.

Acknowledgment. Partial funding was provided by the Air Force Office of Scientific Research and the Air Force Research Laboratory, Materials and Manufacturing Directorate. R.K. thanks the Robert A. Welch foundation for support of the research described here. The authors also acknowledge the help of F. Yeh (in-situ SAXS and WAXS experiments at Brookhaven National Laboratory) and helpful discussions with D. Hunter, Zhi-Gang Wang, and Benjamin S. Hsiao. The Advanced Polymers Beamline is supported by DOE (DE-FG02-99ER 45760) and the APPRT.

Supporting Information Available: Brief summary of current literature on nylon-6 nanocomposite crystallization. This material is available free of charge via the Internet at http://pubs.acs.org.

References and Notes

(1) *Fillers and Filled Polymers*; Gerard, J.-F., Meisel, I., Kniep, C. S., Spiegel, S., Grieve, K., Eds.; Wiley and Sons: New York, 2001.
(2) Arnoldi, D.; Pauli, I.; Nun, E. DE4435157 Thermoplastic Injection Moulding materials with Low Deformation and Isotropic Shrinkage Properties, April 4, 1996.
(3) Vaia, R. A.; Lincoln, D. Mesoscopic Struture of Polymer-Inorganic Nanocomposites. *ACS Symp. Ser.* **2002**, *804*, 99.
(4) Kojima, Y.; Usuki, A.; Kawasumi, M.; Okada, O.; Fukushima, Y.; Kurachi, T.; Kamigaito, O. *J. Mater. Res.* **1993**, *8*, 1185.

(5) Ke, Y.; Long, C.; Qi, Z. *J. Appl. Polym. Sci.* **1999**, *71*, 1139.
(6) Liu, L.; Qi, Z.; Zhu, X. *J. Appl. Polym. Sci.* **1999**, *71*, 1133.
(7) Messersmith, P. B.; Giannelis, E. P. *J. Polym. Sci., Part A: Polym. Chem.* **1995**, *33*, 1047.
(8) Akelah, A.; Moet, A. *J. Mater. Sci.* **1996**, *31*, 3589.
(9) Kojima, Y.; Usuki, A.; Kawasumi, M.; Okada, A.; Kurachi, T.; Kamigaito, O. *J. Appl. Polym. Sci.* **1993**, *49*, 1259.
(10) Yano, K.; Usuki, A.; Kurachi, T.; Kamigaito, O. *J. Polym. Sci., Part A: Polym. Chem.* **1993**, *31*, 2493.
(11) Gilman, J. W.; Kashiwagi, T.; Lichtenhan, J. D. *SAMPE J.* **1997**, *33*, 40.
(12) Lincoln, D. M.; Vaia, R. A.; Benson Tolle, T. H.; Brown, J. M. *IEEE Aerospace Conf. Proc.*; Conf. Proc. of 2000 Meeting. IEEE Aerospace Conf. Big Sky, MT, March 18−25, 2000.
(13) Hseih, D.-T.; Lloyd, T. B.; Rutledge, S. K. Int. SAMPE Symp. Proc., Conf. Proc. of 1998 Meeting (part 2 of 2); Vol. 43, no. 2 SAMPE Covina, CA, pp 1170−1171.
(14) Fong, H.; Vaia, R. A.; Sanders, J. H.; Lincoln, D. M.; John, P. J.; Vreugdenhil, A. J.; Bultman, J.; Cerbus, C. A.; Jeon, H. G. *Chem. Mater.* **2001**, *13*, 4123.
(15) Vaia, R. A.; Price, G.; Ruth, P. N.; Nguyen, H. T.; Lichtenhan, J. *Appl. Clay Sci.* **1999**, *15*, 67.
(16) Alexandre, M.; Dubois, P. *Mater. Sci. Eng.* **2000**, *8*, 1.
(17) Structural Characterization of Polymer Layered Silicate Nanocomposites. In *Polymer-Clay Nanocomposites*; Pinnavaia, T. J., Beal, G. W., Eds.; John Wiley and Sons: New York, 2000.
(18) Sur, G. S.; Sun, H. L.; Lyu, S. G.; Mark, J. E. *Polymer* **2001**, *42*, 9783.
(19) Kawasumi, M.; Hasegawa, N.; Kato, M.; Usuki, A.; Okada, A. *Macromolecules* **1997**, *30*, 6333.
(20) Kurokawa, Y.; Yasuda, H.; Oya, A. *J. Mater. Sci. Lett.* **1996**, *15*, 1481.
(21) Yang, F.; Ou, Y.; Yu, Z. *J. Appl. Polym. Sci.* **1998**, *69*, 355.
(22) Bandyopadhyay, S.; Hsieh, A. J.; Giannellis, E. P. *ACS Symp. Ser.* **2002**, *804*, 15.
(23) Sikka, M.; Cerini, L. N.; Ghosh, S. S.; Winey, K. I. *J. Polym. Sci., Part B: Polym. Phys.* **1996**, *34*, 1443.
(24) Lan, T.; Pinnavaia, T. J. *Chem. Mater.* **1994**, *6*, 2216.
(25) Song, M.; Hourston, D. J.; Yao, K. J.; Tay, J. K. H.; Ansarifar, M. A. *J. Appl. Polym. Sci.* **2003**, *90*, 3239.
(26) Vaia, R. A.; Liu, W.; Koerner, H. *J. Polym. Sci., Part B: Polym. Phys.* **2003**, *41*, 3214.
(27) Vaia, R. A.; Liu, W. *J. Polym. Sci., Part B: Polym. Phys.* **2002**, *40*, 1590.
(28) Dudowicz, J.; Freed, K. F.; Douglas, J. F. *J. Chem. Phys.* **2000**, *113*, 434. Kumar, S. K.; Douglas, J. F. *Phys. Rev. Lett.* **2001**, *87*, 8301. Salaniwal, S.; Kumar, S. K.; Douglas, J. F. *Phys. Rev. Lett.* **2002**, *89*, 258301.
(29) VanderHart, D. L.; Asano, A.; Gilman, J. W. *Chem. Mater.* **2001**, *13*, 3796.
(30) Manias, E.; Kuppa, V. *Eur. Phys. J. E* **2002**, *8*, 193.
(31) Giannelis, E. P.; Krishnamoorti, R.; Manias, E. *Adv. Polym. Sci.* **1998**, *138*, 107.
(32) Xie, W.; Gao, Z.; Pan, W.-P.; Hunter, D.; Singh, A.; Vaia, R. A. *Chem. Mater.* **2001**, *13*, 2979.
(33) Xie, W.; Xie, R.; Pan, W.-P.; Hunter, D.; Koene, B.; Tan, L.-S.; Vaia, R. *Chem. Mater.* **2002**, *14*, 4837.
(34) Sheng, N.; Boyce, M. C.; Parks, D. M.; Rutledge, G. C.; Abes, J. I.; Cohen, R. E. *Polymer* **2004**, *45*, 487.
(35) Maiti, P.; Nam, P. H.; Okamoto, M.; Kotaka, T. *Polym. Eng. Sci.* **2002**, *42*, 1864.
(36) Nam, P. H.; Maiti, P.; Okamoto, M.; Kotaka, T.; Hasegawa, N.; Usuki, A. *Polymer* **2001**, *42*, 9633.
(37) Krikorian, V.; Kurian, M.; Galvin, M. E.; Nowak, A. P.; Deming, T. J.; Pochan, D. J. *J. Polym. Sci., Part B: Polym. Phys.* **2002**, *40*, 2579.
(38) Carter, C. M. *Annu. Tech. Conf.—Soc. Plast. Eng.* **2001**, *3*, 3210.
(39) Ke, Y.; Long, C.; Qi, Z. *J. Appl. Polym. Sci.* **1999**, *71*, 1139.
(40) Tseng, C.-R.; Wu, S.-C.; Wu, J.-J.; Chang, F.-C. *J. Appl. Polym. Sci.* **2002**, *86*, 2492.
(41) Wu, H.-D.; Tseng, C.-R.; Chang, F.-C. *Macromolecules* **2001**, *34*, 2992.
(42) Gelfer, M. Y.; Sics, I.; Liu, L.; Choi, W.-J.; Wang, G. Z.-G.; Vaia, R. A.; Kim, S.-C.; Chu, B.; Hsiao, B. S. *Polym. Mater. Sci. Eng.* **2002**, *86*, 427.
(43) Strawhecker, K.; Manias, E. *Chem. Mater.* **2003**, *15*, 844.
(44) Strawhecker, K.; Manias, E. *Chem. Mater.* **2000**, *12*, 2943.
(45) Han, B.; Ji, G.; Wu, S.; Shen, J. *Eur. Polym. J.* **2003**, *39*, 1641. Yu, Z. Z.; Yang, M.; Zhang, Q.; Zhao, C.; Mai, Y.-W. *J. Polym. Sci., Part B: Polym. Phys.* **2003**, *41*, 1234. Liu, X.; Wu, Q.; Berglund, L. A. *Polymer* **2002**, *43*, 4967.
(46) Liu, Z.; Zhou, P.; Yan, D. *J. Appl. Polym. Sci.* **2004**, *91*, 1834. Zhang, G.; Yan, D. *J. Appl. Polym. Sci.* **2003**, *88*, 2181. Wang, L.-y.; He, S.-q.; Hao, L.-c.; Zhu, C.-s.; Qi, Z.-n. *Gaofenzi Cailiao Kexue Yu Gongcheng* **2002**, *18*, 62.
(47) Wu, Z.; Zhou, C.; Zhu, N. *Polym. Testing* **2002**, *21*, 479.
(48) Lincoln, D. M.; Vaia, R. A.; Wang, Z.-G.; Hsiao, B. S.; Krishnamoorti, R. *Polymer* **2001**, *42*, 09975.
(49) Liu, X.; Wu, Q.; Berglund, L. A.; Qi, Z. *Macromol. Mater. Eng.* **2002**, *287*, 515.
(50) Wu, T.-M.; Chen, E.-C.; Liao, C.-S. *Polym. Eng. Sci.* **2002**, *42*, 1141.
(51) Devaux, E.; Bourbigot, S.; El Achari, A. *J. Appl. Polym. Sci.* **2002**, *86*, 2416.
(52) Wu, T.-M.; Wu, J.-Y. *J. Macromol. Sci., Phys.* **2002**, *B41*, 17.
(53) Fornes, T. D.; Paul, D. R. *Polymer* **2003**, *44*, 3945.
(54) Wu, Q.; Liu, X.; Berglund, L. A. *Macromol. Rapid Commun.* **2001**, *22*, 1438.
(55) Mathias, L. J.; Davis, R. D.; Jarrett, W. L. *Macromolecules* **1999**, *32*, 7958.
(56) Ito, M.; Mizuochi, K.; Kanamoto, T. *Polymer* **1998**, *39*, 4593.
(57) Usuki, A.; Kojima, Y.; Kawasumi, M.; Okada, A.; Kukushima, Y.; Kurauchi, T.; Kamigaito, O. *J. Mater. Res.* **1993**, *8*, 1179.
(58) Krishnamoorti, R.; Giannelis, E. P. *Macromolecules* **1997**, *30*, 4097.
(59) Cho, J. W.; Paul, D. R. *Polymer* **2001**, *42*, 1083.
(60) Lincoln, D. M.; Vaia, R. A.; Wang, Z.-G.; Hsiao, B. S. *Polymer* **2001**, *42*, 1621.
(61) Hsiao, B. S.; Gardner, K. H.; Wu, D. Q.; Chu, B. *Polymer* **1988**, *29*, 1745.
(62) European Molecular Biological Lab., EMBL-Grenoble, and Rapp, G.; Gabriel, A.; Dosiere, M.; Kock, M. H. *J. Nucl. Inst. Methods Phys. Res. A* **1995**, *357*, 178.
(63) Vainshtein, B. K. *Diffraction of X-rays by Chain Molecules*; Elsevier: New York, 1966.
(64) Characteristic peaks for α phase at room temperature are indexed as 200 ($d_{200} \sim 0.440$ nm; $2\theta_{\lambda=0.154\ nm} = 21°$; $2\theta_{\lambda=0.1307\ nm} = 17.8°$), and 002/202 ($d_{002+202} \sim 0.370$ nm; $2\theta_{\lambda=0.154\ nm} = 24°$; $2\theta_{\lambda=0.1307\ nm} = 20.3°$) reflections.[65] Characteristic peaks for the γ phase at room temperature are indexed as 001 ($d_{001} \sim 0.413$ nm; $2\theta_{\lambda=0.154\ nm} = 22°$; $2\theta_{\lambda=0.1307\ nm} = 18.6°$) and 200/201 ($d_{001} \sim 0.386$ nm; $2\theta_{\lambda=0.154\ nm} = 23°$; $2\theta_{\lambda=0.1307\ nm} = 19.5°$), where the latter is a weak shoulder on the former that is normally not resolved.
(65) Arimoto, H.; Ishibashi, M.; Hirai, M.; Chatani, Y. *J. Polym. Sci., Part A* **1965**, *3*, 317. Murthy, N. S.; Aharoni, S. M.; Szollosi, A. B. *J. Polym. Sci., Part B: Polym. Phys. Ed.* **1985**, *23*, 2549.
(66) Ramesh, C.; Bhoje Gowd, E. *Macromolecules* **2001**, *34*, 3308.
(67) Murthy, N. S.; Curran, S. A.; Aharoni, S. M.; Minor, H. *Macromolecules* **1991**, *24*, 3215.
(68) The half-crystallization times reported here are calculated as $(t_{end} - t_{start})/2$, where t_{end} is the end of the primary crystallization regime and t_{start} is the induction time.

MA049768K